RHex-SLIP: A Model of the Robotic Hexapod RHex in the Sagittal Plane

Justin Seipel[1], Pei-Chun Lin[2] and Philip Holmes[3,4]

[1] Department of Integrative Biology,
University of California, Berkeley. Berkeley, CA 94720, U.S.A.
jseipel@berkeley.edu
[2] Department of Electrical and Systems Engineering,
University of Pennsylvania. Philadelphia, PA 19104, U.S.A.
[3] Department of Mechanical and Aerospace Engineering,
[4] Program in Applied and Computational Mathematics,
Princeton University. Princeton, NJ 08544, U.S.A.

November 30, 2006

Abstract

The spring-loaded inverted pendulum (SLIP) is a simple, passively-elastic two-degree-of-freedom model for legged locomotion that describes the saggital-plane center of mass (COM) dynamics of many animal species and some legged robots. In previous work we have extended SLIP to model three-dimensional COM motions and to incorporate multiple stance legs [1, 2]. To better understand the agile hexapedal robot RHex, here we incorporate key details of leg design and motor specifications into SLIP, allowing us to match SLIP gaits with experimental data from RHex, and to investigate their stability properties. We find that motor and leg characteristics, and leg touchdown and liftoff protocols, can significantly influence stability, and that non-periodic "chaotic" gaits can occur.

KEYWORDS: legged locomotion, spring loaded inverted pendulum, hexapedal robot, multiple legs, periodic gait, Poincaré map, stability.

1 Introduction: RHex and SLIP

The robotic hexapod (RHex), shown in Figure 1(a), is a highly dynamic, legged robot [3]. It reaches speeds over 2.5 meters (five body lengths) per

second [4], with ballistic flight phases in which all legs lose contact with the ground: see the idealized running gait in Figure 2. RHex employs six independent motors driving compliant legs that track an alternating double-tripod gait reference signal via proportional-derivative (PD) control [3]. Otherwise, the machine is open-loop: foot contacts with the ground produce reaction forces that drive the body forward with no feedback of leg forces or state variables other than the mechanical reactions themselves. Figure 3 shows a system diagram. Variations on the basic RHex design exist (see Figure 6 below), and a smaller educational version of RHex is currently being developed [5].

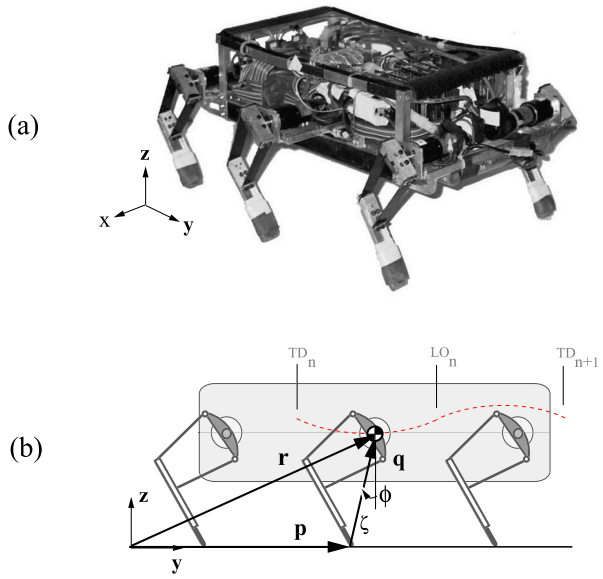

Figure 1: (a) The hexapedal robot RHex and (b) the sagittal-plane RHex-SLIP model. Note inertial coordinate system in (a, b), and that the configuration of only the middle leg acting at the COM is defined in (b); since body pitching is ignored, all three stance legs remain parallel and act effectively as one. This simplifying constraint is further described in Section 2.

RHex's double-tripod gait and control scheme is inspired by the similarly dynamic and robust cockroach *Blaberus discoidalis* [3, 6], which also appears to rely mainly on mechanical "preflexive" reaction forces to stabilize high speed motions (see [7] for an extensive review of legged locomotion and further discussions of control strategies).

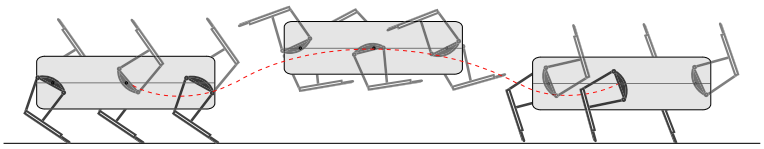

Figure 2: Idealized kinematics of RHex in the sagittal plane, showing the alternating tripod gait in fast running with flight phases.

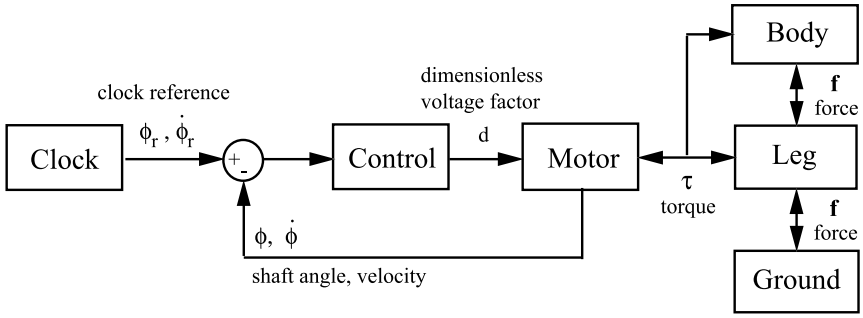

Figure 3: System diagram showing the clock, controller and a detailed representation of the mechanical subsystem. Feedback loops exist within the robot-ground system via force and/or torque reactions among motor, body, legs, and ground: shown by double-sided arrows. A further feedback loop is implemented to feed encoder measurements of leg position to a proportional derivative controller which attempts to track a clock reference.

RHex can traverse varied terrains at speeds unreachable by comparable legged machines. Yet, we still do not fully understand how it interacts with the ground to produce such motions, why certain parameters give locally optimal—high speed, low power—gaits, or how it compares with its biological inspiration, the cockroach. Further, we cannot predict RHex's behavior well enough to derive even simple control laws for stride-to-stride implementation: it remains an essentially feedforward device. This paradigm works well in many conditions and within it, significant improvements in performance have been made by experimental gait adaptation [4]. However, such procedures are tedious and time-consuming, have not provided enough insight to categorize behavior, and cannot predict behaviors beyond local

parameter variation. Systematic design optimization and the addition of feedback control could extend operating ranges, permit complex maneuvers, and allow adaptive behavior. This will require sufficiently detailed models, but ones more tractable than full rigid body simulators [3], which have too many degrees of freedom and parameters to afford much insight or allow systematic continuation and bifurcation studies.

RHex's center of mass (COM) motions are similar to those of running animals, and both can be reproduced rather well by the spring-loaded inverted pendulum (SLIP) [8, 9]: a mass bouncing along atop a passive massless spring [10, 11]. The SLIP is appealingly simple, and while it is still a non-integrable, hybrid dynamical system, approximate analytical solutions can guide parameter studies [12, 13]. The dynamics of a robot or organism that approximates conservative spring-like properties and fixed leg placement at touchdown (TD) might be adequately represented by the SLIP and three-dimensional generalizations of it [1, 2]. Raibert-style hopping robots [14], in particular, share the SLIP morphology: a single axially-sprung leg with leg placement actuation. The SLIP is perhaps also adequate to describe dynamic forces on the COM in steady gaits, and thus may offer a framework for collecting and comparing steady-state data from biological and robotic runners.

However, the SLIP cannot answer stability and perturbation questions for RHex and so cannot serve as a plant model for control purposes; indeed, stable SLIP gaits do not exist for parameter ranges appropriate to RHex. In feed-forward SLIP the leg is held at a fixed angle for touchdown (TD); in RHex, legs cycle continuously following a time-based clock reference and thus can adopt different TD orientations if perturbed, unlike those of SLIP. This certainly changes responses to perturbations quantitatively, but it can also change them qualitatively and alter stability types, as in swing-leg retraction schemes [15, 16, 17]. Earlier work has shown that detailed motor torque production and joint compliance models are necessary to predict gait stability of a quadrupedal robot [18, 19], and we find that similar effects, along with damping in the legs, can also play important roles in the dynamic response of RHex.

In this paper we begin to develop a qualitatively correct and quantitatively sufficiently-close model—a *dynamic template* [20]—which will enable us to better understand legged locomotion and will provide sufficient predictive power for robot control on a stride-to-stride time scale. We propose a sagittal-plane, non-pitching, RHex-SLIP model, with added effects that appear capable of adequately capturing RHex's dynamics. These include a more realistic damped leg-spring model, a clock governing leg position at

TD, torque-limited motors at the hips, and more realistic liftoff (LO) transitions. Figure 1(b) shows a cartoon and kinematic description of RHex-SLIP. Section 2 describes the model and equations of motion, model results are compared with experimental data in Section 3, and we conclude in Section 4.

This "continuation" from SLIP to RHex-SLIP seems reasonable since RHex's stance legs essentially superpose to produce COM motions, and several important effects can be included without introducing rigid body rotations. Our model contrasts with, and is simpler than, the recent study of quadrupedal bounding dynamics of Poulakakis et al. [21], which necessarily includes pitching to capture alternating front and rear leg ground contacts. Both that paper and the present one add to growing evidence that open-loop feedforward control and appropriate electro-mechanical design can produce stable, fast and nimble machines.

2 The RHex-SLIP model

In this section we derive equations of motion for RHex-SLIP. We first describe the clock—an analog of the central pattern generator in animals—that determines the robot's pace and footfall pattern; we then model the passively visco-elastic legs, the proportional-derivative feedback that commands hip torques, and the motor characteristics that determine the actual torques. Decoupling axial and transverse leg forces, and neglecting body rotations, yields relatively simple model equations.

2.1 The clock

The alternating tripod gait of RHex is loosely controlled by a time-based reference trajectory: the *clock*. Each leg is kept near its reference trajectory by an independent motor following a proportional-derivative control law. In alternating tripod gaits a full stride consists of left and right half-strides or stance phases. Legs must generally rotate more slowly during stance than in flight since stance occupies less than half a full leg revolution and the legs cycle—rotating continuously in the same sense—to return to stance. To achieve this, RHex's clock uses a piece-wise linear angle vs. time reference trajectory characterized by four parameters: the total stride or cycle period t_c, the duty factor (the ratio of a single stance period over the cycle period) t_s/t_c, the leg angle swept during stance ϕ_s, and an angle offset to break symmetry in the gait ϕ_o: see Figure 4.

Although remaining approximately in synchrony with the desired clock phase during steady-state operation, RHex's actual leg positions differ from

the clock reference. RHex is designed to use these deviations during stance to purposefully generate responsive torques through proportional derivative (PD) control, thus propelling itself forward. This approach intentionally uses the dynamic response of a conventional trajectory controller to benefit the whole system: its goal being not to track leg trajectories but to generate stable forward motion.

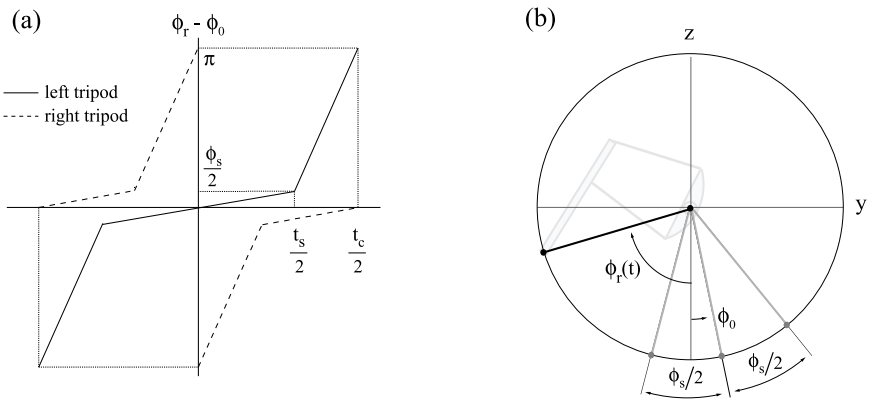

Figure 4: (a) The "clock" reference: desired leg angles vs. time, and (b) the corresponding desired leg configuration. Both (a) and (b) are defined by the clock parameters $(t_c, t_s, \phi_s, \phi_o)$, as described in the text. Note that in (b), the coordinates (y, z) refer to the body frame, but since rotations are neglected, their directions coincide with the inertial frame of Figure 1(b).

2.2 The leg and motor models

During stance, with legs compressed and motor torques applied at the hips, forces acting on a leg are related by the free-body diagram of Figure 5(a). Since the legs are light relative to the body (An individual leg is less than 2% of total mass)[1], we neglect leg mass and assume force balance across each leg at every instant throughout the body's trajectory. RHex's COM lies within 1% of the axis of the shafts driving the middle hips, and to proceed further we shall assume that it *coincides* with this axis. As shown in Section 2.3,

[1]Leg masses range from 50 to 150 grams per leg. The carbon fiber semi-circle leg shown in Figure 6 is typically lighter ($\approx$ 50 grams), whereas the four-bar leg of Figure 1 ranges from 100 to 150 grams (with diagnostic instruments attached). Total mass is $\approx$ 8 kg.

this and our neglect of pitching allows us to superpose all forces at the COM (Figures 5(b, c)), and so we only give detailed equations for the middle leg.

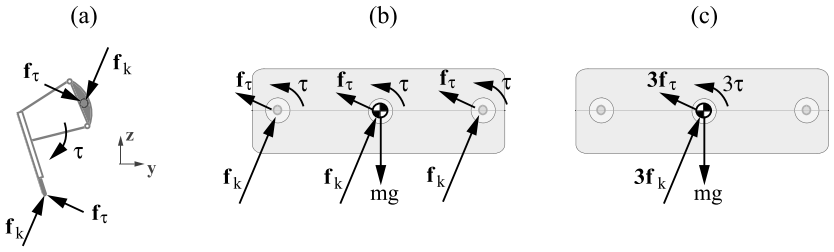

Figure 5: Free body diagrams for (a) a single leg, (b) the rigid body, and (c) reduction to a net resultant force acting at the COM (effectively the same as three times a single leg).

The force vector $\mathbf{f}_k$ lies along the axis from foot to hip, and is primarily due to passive spring and damping properties in the leg: see [22]. The force vector $\mathbf{f}_\tau$ is perpendicular to the foot-hip axis, and is mostly due to motor torque applied at the hip and transmitted to the foot through the leg, which is assumed sufficiently stiff normal to $\mathbf{f}_k$ to remain undeformed in this direction. Assuming that during stance the foot is fixed in the inertial frame, and referring to the kinematic relationships shown in Figure 1(b), we obtain the following leg configuration at each instant during stance:

$$\mathbf{p} = \text{constant}\,, \quad \mathbf{q} = \mathbf{r} - \mathbf{p}\,, \tag{1}$$

$$\zeta := |\mathbf{q}|\,, \quad \dot{\zeta} = \frac{q_y\dot{q}_y + q_z\dot{q}_z}{\zeta}\,, \tag{2}$$

$$\phi := \tan^{-1}\left(\frac{q_y}{q_z}\right), \quad \dot{\phi} = \frac{q_z\dot{q}_y - q_y\dot{q}_z}{q_z^2\sec^2\phi}\,. \tag{3}$$

Minimal forces act on legs during swing, and so we assume that, following lift-off, their configuration instantaneously matches that specified by the clock reference and motor controller at the hip:

$$\mathbf{q} = \zeta_o(\sin\phi_r, \cos\phi_r)\,, \tag{4}$$

where ζ_o is the uncompressed leg length.

A spring law: In addition to the four-bar linkage leg shown on RHex in Figure 1, versions have also been built with semicircular legs, as in Figure 6

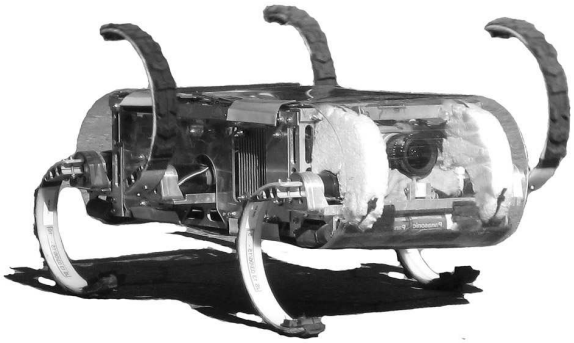

Figure 6: RHex with semi-circular legs constructed with carbon fiber composites and synthetic tire-rubber tread. Photo courtesy Kod*lab http://kodlab.seas.upenn.edu/ResearchPage/.

(also see the insets in Figure 7). The rolling ground contact substantially complicates the mechanics—it provides a distributed, moving foot force and a variable moment arm—and we do not explicitly model such a leg here, although we shall compare the RHex-SLIP model with RHex with semi-circle legs at one operating point due to a lack of four-bar experimental data (see Figure 10), and we use semi-circle leg data in deriving our spring law. Both leg designs employ reinforced fiber composites for compliance and energy storage, and, while the four-bar design produces primarily radial deformations [22], both it and the semi-circle form couple the force components of Figure 5(a) in a complex manner. Nontheless, we shall assume that the radial force $\mathbf{f}_k$ along the radial foot-hip axis is solely due to passive elasticity and damping, and that the tangential force $\mathbf{f}_\tau$ is solely due to hip torque. While this is adequate to reproduce RHex data, more realistic leg models may be necessary for design and optimization purposes.

We represent the effects of leg elasticity and damping by a simple linear spring and damper in parallel. This permits a reasonable fit to experimental observations, as shown in Figure 7. The data points were estimated from semi-circle and four-bar leg strain measurements of Moore [23, Chap. 4], normalized to the same unloaded leg length. In these experiments the hip was fixed and the "toe" displaced over a rectangular grid while radial and tangential foot forces were measured. It is not clear how best to extract effective radial forces $\mathbf{f}_k$ from this data. For example, stance legs slip when tangential forces become too high in comparison to radial forces, so only

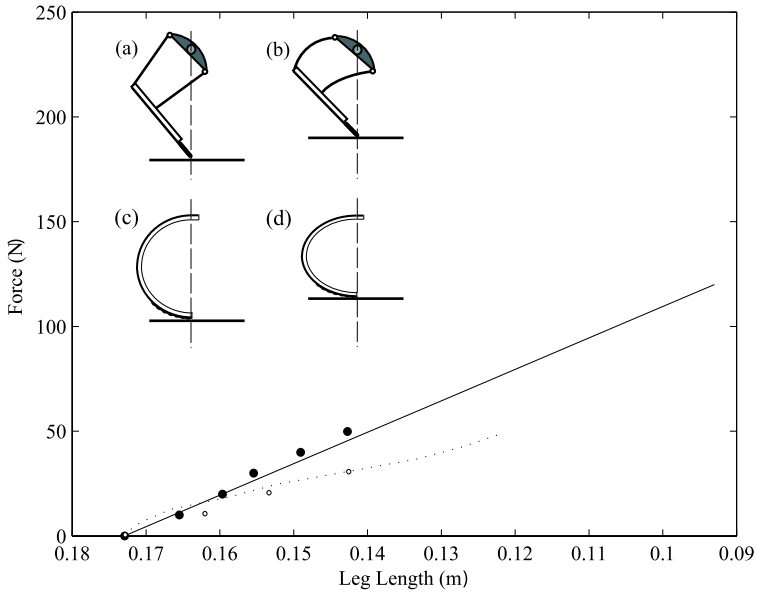

Figure 7: The linear spring model (solid) and force-radial displacement data for both four-bar (dotted) and semi-circle legs (open and closed circles). The linear spring stiffness is given in Table 1. Insets show (a) uncompressed and (b) compressed four-bar legs; semi-circle legs are shown in (c) and (d).

data lying within a friction cone is relevant [22, Appendix III]. We fitted our spring law to radial force data as the toe is displaced radially toward the hip, which we believe best represents the working region (solid circles in Figure 7). The open circles and dotted curve were obtained by moving along toe-displacement curves on which the hip torque is zero: these indicate a softening spring, although the four-bar curve does turn up slightly at large strains.

Specifically, the total force magnitude along the leg is modeled as

$$f_k = k\,(\zeta_o - \zeta) - c\,\dot{\zeta}\,, \tag{5}$$

where ζ and ζ_o are the compressed and uncompressed leg lengths, and k and c are the spring and damping coefficients. The force vector along the leg immediately follows:

$$\mathbf{f}_k := f_k \frac{\mathbf{q}}{\zeta}\,. \tag{6}$$

Spring and damping values are given in Table 1.

Parameter	Value	Units
g, gravitational constant	9.8	m/s^2
m, body mass	7.0	kg
ζ_o, unloaded leg length	0.17	m
k, linear spring constant from [24, 3]	1500	N/m
c, linear damping constant	17.5	Ns/m

Table 1: Physical parameters. Mass, motor, and leg parameters are taken from [3] and [24].

A motor model: From Figure 5 the force vector $\mathbf{f}_\tau$ perpendicular to the leg is determined by the torque τ applied at the hip:

$$\mathbf{f}_\tau = \frac{\tau}{\zeta^2}[q_z, -q_y]\,. \tag{7}$$

To describe the motor torques τ we use the physics-based model first derived in [25], to which the reader should refer for further details. A brief description follows.

The output torques generated by RHex's [3] direct-current motors depend on the applied voltage and angular velocity $\dot{\phi}$ of the motor shafts. The voltage applied to each motor is specified by the following PD control law:

$$V_{pd} = K_p(\phi - \phi_r) + K_d(\dot{\phi} - \dot{\phi}_r)\,, \tag{8}$$

where ϕ_r and $\dot{\phi}_r$ are the clock references of Figure 4, ϕ and $\dot{\phi}$ denote the actual shaft motions, and K_p and K_d are proportional and derivative control gains respectively. However, the voltage applied by the onboard amplifier cannot exceed that of the power supply $\pm V_s$, and the effective resistance of the amplifier seen by the motor circuit depends on the relative magnitude of voltage at the amplifier-motor terminals. Therefore, as in [25], it is convenient to define a dimensionless voltage or *duty factor* that depends on applied voltage V_{pd}:

$$d = \text{sign}(V_{pd}) \times \min\left\{1\,, \frac{|V_{pd}|}{25}\right\}. \tag{9}$$

Under the assumption that the electro-mechanical motor dynamics is sufficiently fast compared to the body/leg dynamics of RHex, the torque supplied at each hip can then be modeled as in [25], in which the motor output torque is specified as a function of duty factor d and shaft velocity

$\dot{\phi}$:

$$\tau = \eta N K_t \left(\frac{dV_s - K_s \dot{\phi}}{R_a + d^2 R_{amp}} \right). \tag{10}$$

The motor parameters $(N, \eta, K_t, V_s, K_s, R_a, R_{amp})$ are defined in Table 2.

Constant	Value	Units
N, gear ratio	33	-
η, motor-gear efficiency	0.80	-
V_s, source voltage	25	V
R_a, armature(motor) resistance	1.65	V/A
R_{amp}, amplifier resistance	0.44	V/A
K_t, conversion factor	0.0160	Nm/A
K_s, conversion factor	0.625	Vs

Table 2: Physical motor constants given in [25]. K_s is implicitly given by experimental data plotted in [25, Fig. 7] and reproduced in Figure 8, but further details provided by [5] were necessary to clarify the mapping from the proportional-derivative controller voltage (8) to the dimensionless voltage factor d (9).

Equations (8-10) describe the motor model, and its accuracy is illustrated in Figure 8, in which the predicted torque is shown along with experimental data reproduced from [25, Fig. 7]. The experimental data is produced by coupling the shaft of the RHex motor to that of a more powerful motor, which attempts to run the whole system at several fixed angular velocities, while the duty factor d is varied from zero to one and back. The torque is measured using a torque transducer. The straight lines predicted by the model (10) are produced by fixing the duty factor at the values indicated and varying $\dot{\phi}$. The experimental data fits nicely between the lines $d = 0$ and $d = 1$. See [25] for further explanation of this data. We note that several steps involving analog-to-digital conversion, scaling and offset factors combine to create negligible effects and are therefore omitted from the model [5].

2.3 Equations of motion

Our model assumes that the COM coincides with the middle hip axis, the legs of each tripod remain in synchrony during flight (since they follow identical references), and the body is not allowed to rotate. TDs therefore occur simultaneously, all three legs maintain identical configurations, and COM moments due to front and rear leg forces cancel (Figure 5(b)). The motor

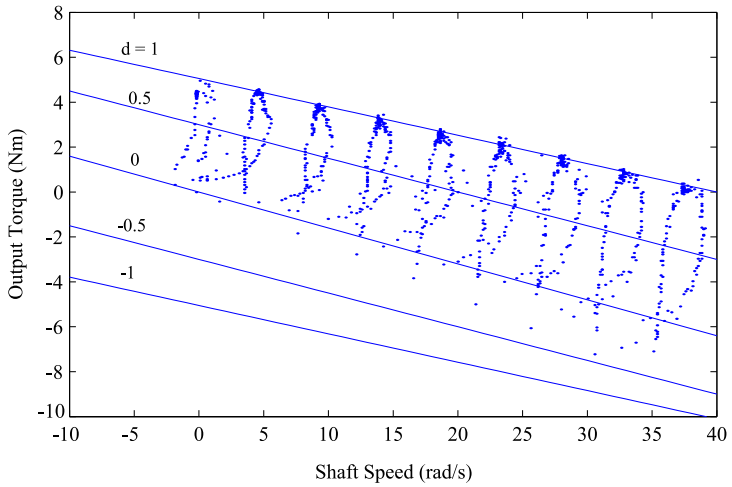

Figure 8: Output torque versus shaft speed for the Maxon RE118751, 20 Watt DC Motor (points), reproduced from [25]). Lines show predictions of Equation (10) (solid) for several values of the dimensionless voltage factor d. The 33:1 gear ratio used to increase torque transmitted to the leg is taken into account (Maxon 114473 planetary gear).

torques, however, combine to produce a net moment that would pitch the body up during stance[2], so our neglect of body rotations may be the weakest point in the following analysis. (In essence, we assume that the pitching moment of inertia is large compared with motor torques.) However, it allows us to add the forces to produce one effective leg at the COM: Figure 5(c), as in the simpler RHex model of [2], and it produces acceptable results for COM translation dynamics. The total resultant force acting on the COM, for one tripod, is then

$$\mathbf{f} = 3\left(\mathbf{f}_k + \mathbf{f}_\tau\right) . \tag{11}$$

The free body diagrams in Figure 5 are shown for a single tripod gait in contact with ground, however, the left and right tripods (all six legs) may simultaneously make ground contact during a double-stance phase, which is common in walking gaits. Conversely, flight phases, in which only gravity acts on the body ($\mathbf{f} = \mathbf{0}$) and motions are ballistic, occur in running gaits.

The equations of motion for COM translations are, by Newton's second

[2]RHex clearly exhibits such behavior, the rear legs bearing the greatest loads and doing the most work [5].

law:

$$\ddot{\mathbf{r}} = \frac{1}{m}\sum_{j=1}^{2} \mathbf{f}_j - g\hat{\mathbf{e}}_z \,, \tag{12}$$

where $\hat{\mathbf{e}}_z = (0, 1)$, and $\mathbf{f}_j$ is the net resultant force for the jth tripod. Here $j = 1$ for the left tripod and $j = 2$ for the right, though the distinction is irrelevant for this sagittal-plane model. The important thing to notice here is the hybrid nature of the system: four different vector fields occur in (12), depending on the combinations of tripods in stance and flight (both, one, the other, or neither tripod in stance). Switching among them is determined by the following functions:

$$s_j^{TD} := z - \zeta_o \cos\phi_j \,, \tag{13}$$

$$s_j^{LO} := f_{z,j} - mg \,. \tag{14}$$

When $s_j^{TD} = 0$ and $\dot{s}_j^{TD} < 0$, touchdown (TD) occurs. Likewise, when $s_j^{LO} = 0$ and $s_j^{LO} < 0$, liftoff (LO) occurs. Upon touchdown, the vector $\mathbf{p}_j$ is fixed. The leg vector $\mathbf{q}_j$ follows from (1) and $\mathbf{f}_j$ is given by (6). When the jth tripod lifts off the ground, then $\mathbf{f}_j = \mathbf{0}$ and the leg vector $\mathbf{q}_j$ is governed by the clock: see (4).

3 Results

Numerically integrating the hybrid system defined in Equations (12-14) for clock parameters and control gains typical of slow running (jogging) behavior in RHex, we find stable periodic solutions in agreement with experimental observations. These stable gaits are robust, like those of the physical system, having relatively large domains of attraction compared with the small ones of the SLIP [11]. Perturbations to apex velocity of well over 50% do not deter the system from returning to steady locomotion, and substantial deviations are often corrected within 1-3 strides. Figure 9 (top) shows behavior at steady-state, and Figure 9 (bottom) shows a sagittal plane trajectory settling on a steady gait after an initial perturbation, compared with an experimental run with the same parameter values. A perturbation from steady-state motion of 0.4 m/s in velocity magnitude, 0.4 rad in velocity heading, and 0.04 sec to the reference clock was applied at the beginning of the run (at TD) in the latter case: see Section 3.1 for a description of stability calculations and the related stride map.

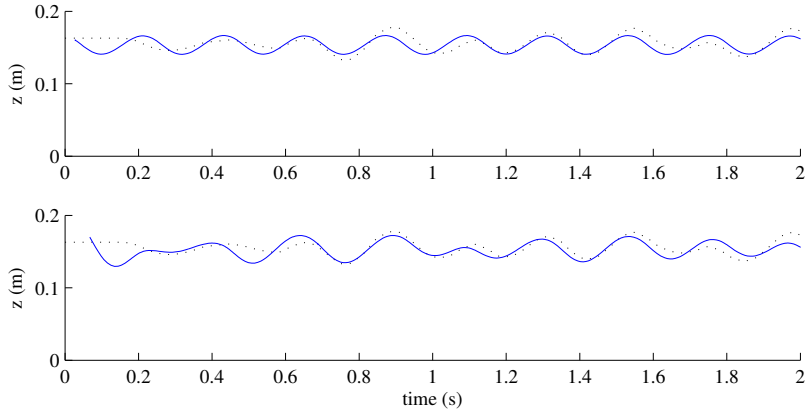

Figure 9: Comparisons of steady-state (top) and transient (bottom) model solutions (solid) with experimental data from RHex (dotted), for the jogging gait of Figure 10 and Table 3. These plots of z vs. t shows close agreement in stride frequency, but model stride lengths can deviate significantly from experimental values, leading to the discrepancies in average velocities plotted in Figure 10.

3.1 Behavior over a range of speeds

The model was run at four points in the parameter space, representing different gaits, with clock and gain parameter values given in Table 3. For each point we compute average speed and compare model predictions with experimental values approximated from video-capture of quasi-steady trajectories. As shown in Figure 10, the model exhibits the appropriate stable dynamics at all points, satisfying the first requirement of a dynamic template, and it also predicts average speed acceptably at three of them. The exception is the fast run with semi-circle legs, which we do not expect to agree well with four-bar results since its rolling foot contact involves very different mechanics.

In Figure 10 we also plot curves from two simple predictive, but not dynamic, theories. The first and most naive predicts the average velocity as proportional to the clock frequency: $\langle v \rangle = \frac{C}{t_c}$. The proportionality constant can be chosen to optimize overall fit, or to match the curve at one operating point. In this case, $C = 0.3$ was chosen to find a fit between walking and jogging operating regions ($t_c \in (0.4, 0.9)$). This does quite well overall, except for high speed running. The second theory includes more clock parameters

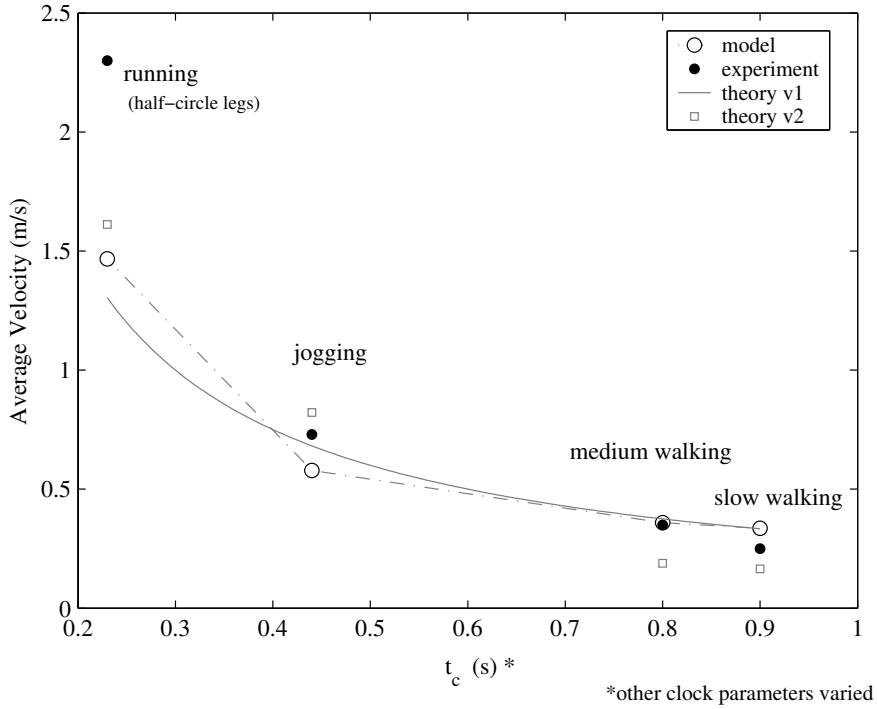

Figure 10: Comparison of the model's behavior (open circles connected by dash-dot line) with that of the physical robot (filled black circles) at four operating points with parameter values of Table 3. Also plotted are values from two simple predictive theories described in the text.

and relies on the assumption that average speed is approximately equal to that of the idealized clock gait: $\langle v \rangle = (\text{stance distance})/(\text{stance period})$. The resulting expression can be simplified further for $\phi_o = 0$ (symmetric stance phases) to yield $\langle v \rangle \approx \frac{2\zeta_o}{t_s} \sin(\frac{\phi_s}{2})$. Its predictions are shown by squares since different clock parameters are used at each point, whereas the first theory uses only t_c and so a curve can be plotted in the ($\langle v \rangle$,t_c) projection of the higher-dimensional parameter space.

These simple predictive theories perform fairly well, and seemingly challenge the usefulness of a more complicated, dynamic model of RHex. However, they are merely telling us that for a gait which exists, a priori, the actual stride/stance periods and geometry are close to those of the clock reference. This is intuitive: we already know that the clock period t_c and

gait	t_c sec	t_s/t_c	ϕ_s rad	ϕ_o rad	K_p V/rad	K_d Vs/rad	$\langle v \rangle$ m/s
slow walking	0.9	0.69	0.60	-0.15	24.0	0.67	0.34
medium walking	0.80	0.69	0.61	-0.15	24.0	0.67	0.36
jogging	0.23	0.32	0.70	0.22	34.2	1.19	0.58
running	0.44	0.39	0.84	0.10	18.4	0.42	1.47

Table 3: Clock parameters and proportional-derivative controller gains for the model and RHex at four characteristic operating points. Average forward speeds ($\langle v \rangle$ m/sec) of RHex are also shown.

actual stride period must match for a periodic gait. Further, the simple predictive theories do not reveal the causal dynamics and so cannot predict existence or stability of gaits for arbirary clock parameters, though other geometrical theories might help exclude periodic gaits for certain parameter ranges based on simple physical constraints; for example, upper limits on motor power and thus shaft speed would rule out the existence of gaits below some critical stride period. However, in general, a dynamical model is required to provide a full range of predictive capabilities, and to investigate and understand fundamental causes, interactions, and effects. Only then can more insightful robot design and more systematic control be applied.

Stability of periodic gaits: We define a stride-to-stride Poincaré return map **P**, which evolves the system from left tripod TD to the next left tripod TD. The model has two translation degrees of freedom and so has a 4-dimensional phase space both in stance and flight (cf. Section 2.3).

Since the Poincaré cross section effectively fixes one dimension via TD leg angle, orbits of **P** can be described by three or four variables. For gaits with single (tripod) stance phases we choose COM velocity magnitude and direction and TD time (v, δ, t). When double stance phases occur, as in walking, we must also track the right tripod position at left tripod touchdown. The double stance map therefore evolves (v, δ, t, p_y) forward from left tripod touchdown to touchdown, where the fore-aft foot position p_y of the right tripod is included. (We may assume that $p_z = 0$, since the foot is on the ground.)

Following the methods of [1, 2] we then approximate eigenvalues of the linearized map **DP** by finite-differencing results from numerical simulations started at and near fixed points corresponding the periodic gaits. For the four gaits of Figure 10 we obtain the eigenvalues shown in Figure 11. All the eigenvalues have magnitudes less than one, implying asymptotic stability [26,

27], and the magnitudes for walking gaits are significantly smaller than those for jogging and running, differing by an order of ten for slow walking. This may be due to the dominance of static stability at low speeds and the relatively large motor torques in that regime, which can entrain the mechanical system.

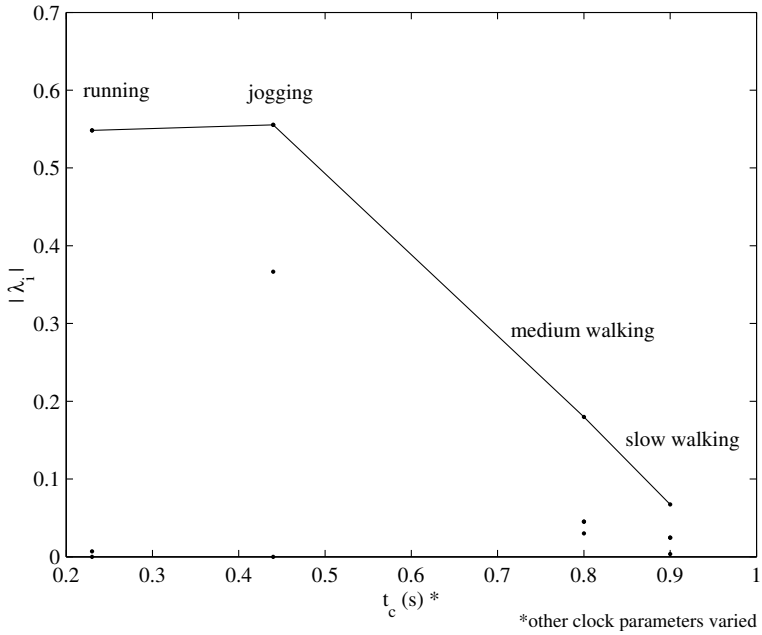

Figure 11: Eigenvalue magnitudes of the stride map evaluated at the operating points of Figure 10. The dashed line connects maximum magnitudes at each operating point, illustrating increasing stability in moving from running to walking. For running, the stride map has three eigevalues; for walking, four (fewer points may appear as some eigenvalues are complex conjugates that share the same absolute value).

3.2 A comment on sensitivity to liftoff conditions

The model's behavior appears robust to perturbations over a substantial parameter range. Indeed, in preliminary studies using a nonlinear hardening leg spring and a different (and less realistic) motor model [28], we found broadly similar dynamical behavior. Nonetheless, some parameters seem more crucial. In particular, changes to LO conditions can affect the nature

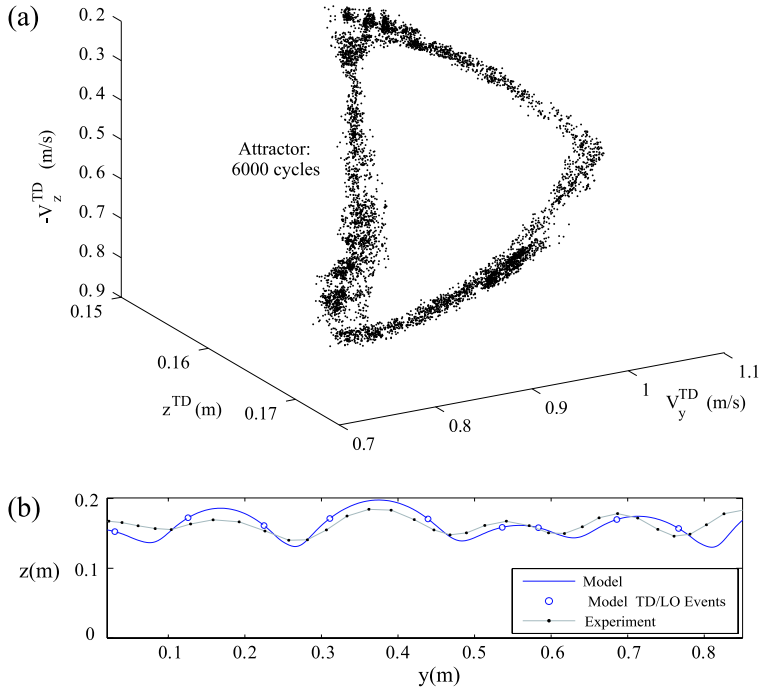

Figure 12: A solution of RHex-SLIP computed for the jogging parameters of Table 3, with the modified LO condition described in Section 3.2: (a) COM velocity and height at TD through 6000 cycles, and (b) a typical gait segment compared with experimental data.

of the attractor: changing it from periodic to quasi-periodic and apparently even chaotic, as illustrated in Figure 12.

Here the LO switching function in the model of [28, Chap. 5] is modified from $s^{LO} = f_z - mg$ of Equation (14), in which LO occurs when the vertical force at the foot drops to zero, to $s^{LO} = f_k$, so that LO occurs when the leg reaches its equilibrium length. This may seem unrealistic for standard RHex on flat terrain since vertical forces can become negative, but it is relevant for irregular or sticky terrain, for legs with spines [29], or for a futuristic RHex with synthetic gecko-hair [30] feet. Tensile forces could be generated in such cases. The resulting gait is robust and appears to be stable in that perturbations are rejected, but the attractor is apparently chaotic. The COM does not return to a previous state in 6000 strides. Figure 12(b)

shows that a segment of this non-periodic solution plotted in the (y, z) plane also compares quite well with experimental data.

Bifurcations from periodic to quasi-periodic motions, or even to chaotic attractors, are common for many kinds of symmetry breaking [26, 27]. Irregular ground and foot contact models, which can strongly influence TD and LO events, can be expected to lead to such such dynamics. Instances in which different LO/TD conditions completely destabilize the gait can also be found.

4 Conclusions

In this paper we develop a simple but appropriately-tailored model of the hexapedal robot RHex, and show that it predicts gaits that agree well with experimental data. This spring-loaded inverted-pendulum (SLIP) model is minimal in that it is restricted to the sagittal plane and neglects pitching motions and leg mass. However, substantial detail must be added to the two mechanical degrees of freedom to correctly predict the dynamics of RHex. In particular, the reference clock that drives leg motors via proportional-derivative feedback must be described and feedback gains specified, the damping and stiffness of the leg springs must be modeled, and motor torque specifications included.

The resulting RHex-SLIP model can predict average speeds over a substantial parameter range, and it correctly captures stable gaits and COM translation motions that have been observed in RHex. It also allows us to numerically derive a low-dimensional stride-to-stride return map, the eigenvalues of which quantify gait stability and predict rates at which perturbations should damp out. While the model is fairly robust, its behavior seems particularly sensitive to changes in liftoff conditions, which can cause bifurcations to non-periodic gaits. This suggests that better touchdown, liftoff and ground contact models are required.

A major defect of the present model is neglect of pitching dynamics, which is known to be significant in RHex [5]. Inclusion of this in a three-degree-of-freedom mechanical system will be an important step in our program to derive relatively simple models with improved explantory and predictive capabilities. Future directions in RHex modeling might also include more detailed leg models (cf. §2.2). Ground contact and friction are clearly also important phenomena that must be incorporated into the model if we are to understand dynamics on realistic terrains [29]. Three-dimensional, rigid-body models of RHex would allow us to investigate dynamic coupling

among the degrees of freedom, and might suggest simple passive methods to damp out undesired modes of behavior. Incorporation of novel controllers within such detailed models could also yield improved designs.

Acknowledgements: This work was partially supported by NSF EF-0425878 (Frontiers in Biological Research). Justin Seipel also benefited from an NSF Graduate Fellowship and an IC Postdoctoral Fellowship. We thank Hal Komsuoglu, Dan Koditshek, and other members of Kod*lab for assistance and advice.

References

[1] J. Seipel and P. Holmes. Running in three dimensions: Analysis of a point-mass sprung-leg model. *Int. J. Robotics Research*, 24(8):657–674, 2005.

[2] J. Seipel and P. Holmes. Three dimensional translational dynamics and stability of multi-legged runners. *Int. J. Robotics Research*, 25(9), 2006.

[3] U. Saranli, M. Buehler, and D.E. Koditschek. RHex: A simple and highly mobile hexapod robot. *Int. J. Robotics Research*, 20(7):616–631, 2001.

[4] J.D. Weingarten, G.A.D. Lopes, M. Buehler, R.E. Groff, and D.E. Koditschek. Automated gait adaptation for legged robots. In *Proceedings of the IEEE International Conference On Robotics and Automation*, volume 3, pages 2154–2158, New Orleans, 2004. IEEE.

[5] H. Komsuoglu. Personal communication, 2006.

[6] D.E. Koditschek, R.J. Full, and M. Buehler. Mechanical aspects of legged locomotion control. *Arthropod Structure and Development*, 33 (3):251–272, 2004.

[7] P. Holmes, R.J. Full, D. Koditschek, and J. Guckenheimer. The dynamics of legged locomotion: Models, analyses and challenges. *SIAM Review*, 48(2):207–304, 2006.

[8] R. Blickhan. The spring-mass model for running and hopping. *J. Biomechanics*, 22:1217–1227, 1989.

[9] R. Altendorfer, N. Moore, H. Komsuoglu, M. Buehler, H.B. Brown Jr., D. McMordie, U. Saranli, R.J. Full, and D.E. Koditschek. RHex: A

biologically inspired hexapod runner. *Autonomous Robots*, 11:207–213, 2001.

[10] R. Blickhan and R.J. Full. Similarity in multi-legged locomotion: bouncing like a monopode. *J. Comp. Physiol. A*, 173:509–517, 1993.

[11] R.M. Ghigliazza, R. Altendorfer, P. Holmes, and D. Koditschek. A simply stabilized running model. *SIAM Review*, 47(3):519–549, 2005. Original paper appeared in SIAM J. Applied Dynamical Systems 2(2):187-218, 2003.

[12] W.J. Schwind and D.E. Koditschek. Approximating the stance map of a 2 dof monoped runner. *J. Nonlin. Sci.*, 10(5):533–568, 2000.

[13] H. Geyer, A. Seyfarth, and R. Blickhan. Spring mass running: simple approximate solution and application to gait stability. *J. Theor. Biol.*, 232:315–328, 2005.

[14] M. Raibert. *Legged Robots that Balance*. MIT Press, Cambridge, MA, 1986.

[15] A. Seyfarth, H. Geyer, and H. Herr. Swing-leg retraction: a simple control model for stable running. *J. Exp. Biol.*, 206:2547–2555, 2003.

[16] R. Altendorfer, D.E. Koditschek, and P. Holmes. Stability analysis of legged locomotion models by symmetry-factored return maps. *Int. J. Robotics Res*, 23 (10-11):979–999, 2004.

[17] R. Altendorfer, D.E. Koditschek, and P. Holmes. Stability analysis of a clock-driven rigid-body SLIP model for RHex. *Int. J. Robotics Res*, 23 (10-11):1001–1012, 2004.

[18] I. Poulakakis, J.A. Smith, and M. Buehler. Experimentally validated bounding models for the Scout II quadrupedal robot. In *International Conference on Robotics and Automation*, volume 3, pages 2595–2600. IEEE Press, 2004.

[19] I. Poulakakis, J.A. Smith, and M. Buehler. Modeling and experiments of untethered quadrupedal running with a bounding gait: The Scout II robot. *Int. J. Robotics Res.*, 24 (4):239–256, 2005.

[20] R.J. Full and D.E. Koditschek. Templates and anchors: neuromechanical hypotheses of legged locomotion on land. *J. Exp. Biol.*, 202:3325–3332, 1999.

[21] I. Poulakakis, E. Papadopoulos, and M. Buehler. On the stability of the passive dynamics of quadrupedal running with a bounding gait. *Int. J. Robotics Res.*, 25 (7):669–687, 2006.

[22] P-C. Lin, H. Komsuoglu, and D.E. Koditschek. A leg configuration measurement system for full body pose estimates in a hexapod robot. *IEEE Transaction on Robotics*, 21 (3):411–422, 2005.

[23] E.Z. Moore. Leg design and stair climbing control for the *RHex* robotic hexapod. Master's thesis, McGill University, Montreal, Canada, 2002.

[24] U. Saranli and D.E. Koditschek. Template based control of hexapedal running. In *Proceedings of the IEEE International Conference On Robotics and Automation*, volume 1, pages 1374–1379, Taipei, Taiwan, 2003. IEEE.

[25] D. McMordie, C. Prahacs, and M. Buehler. Towards a dynamic actuator model for a hexapod robot. In *Proceedings of the IEEE International Conference On Robotics and Automation*, volume 1, pages 1386–1390, Taipei, Taiwan, 2003. IEEE.

[26] R.L. Devaney. *An Introduction to Chaotic Dynamical Systems*. Addison Wesley, Reading, MA, 1986.

[27] J. Guckenheimer and P. Holmes. *Nonlinear Oscillations, Dynamical Systems, and Bifurcations of Vector Fields*. Springer-Verlag, New York, NY, 1990.

[28] J. Seipel. *Actuated Models of Multi-Legged Locomotion*. PhD thesis, Princeton University, 2006.

[29] J.C. Spagna, D.I. Goldman, P. Lin, D.E. Koditscheck, and R.J. Full. Distributed mechanical feedback in arthropods and robots simplifies control of rapid running on challenging terrain. To appear, 2006.

[30] K. Autumn, W.P. Chang, R. Fearing, T. Hsieh, T. Kenny, L. Liang, W. Zesch, and R.J. Full. Adhesive force of a single gecko foot-hair. *Nature*, 405:681–685, 2000.